Neutrino induced reactions for ν-process nucleosynthesis of ^{92}Nb and ^{98}Tc

Myung-Ki Cheoun, Eunja Ha, T. Hayakawa, Satoshi Chiba, Ko Nakamura, Toshitaka Kajino, and Grant J. Mathews

Phys. Rev. C **85**, 065807 — Published 21 June 2012

DOI: 10.1103/PhysRevC.85.065807

Neutrino induced reactions for ν-process nucleosynthesis of ^{92}Nb and ^{98}Tc

Myung-Ki Cheoun[1) *], Eunja Ha[1)], T. Hayakawa[2)], Satoshi Chiba[2,3)], Ko Nakamura[4)] Toshitaka Kajino[4,5)], Grant J. Mathews[6)]

1)Department of Physics, Soongsil University, Seoul 156-743, Korea

2)Advanced Science Research Center, Japan Atomic Energy Agency, 2-4 Shirakata-shirane, Tokai, Ibaraki 319-1195, Japan

3)Research Laboratory for Nuclear Reactors, Tokyo Institute of Technology 2-12-1-N1-9 Ookayama, Meguro-ku, Tokyo, 152-8550, Japan

4)National Astronomical Observatory, Mitaka, Tokyo 181-8589, Japan

5)Department of Astronomy, Graduate School of Science, University of Tokyo, 7-3-1 Hongo, Tokyo 113-0033, Japan

6)Center for Astrophysics, Department of Physics, University of Notre Dame, IN 46556, USA

(Dated: May 21, 2012)

* Corresponding author : cheoun@ssu.ac.kr

Abstract

It has recently been proposed that $^{92}_{41}$Nb and $^{98}_{43}$Tc may have been formed in the ν-process. We investigate the neutrino induced reactions related to the ν-process origin of these two odd-odd nuclei. We find that the main neutrino reactions to produce $^{92}_{41}$Nb are the charged-current (CC) ^{92}Zr$(\nu_e, e^-)^{92}$Nb and the neutral-current (NC) ^{93}Nb$(\nu(\bar{\nu}),\ \nu^{'}(\bar{\nu})^{'}$ n $)^{92}$Nb reactions. Similarly, the main reactions for $^{98}_{43}$Tc, are the CC reaction ^{98}Mo$(\nu_e, e^-)^{98}$Tc and the NC reaction ^{99}Ru$(\nu(\bar{\nu}),\ \nu^{'}(\bar{\nu})^{'}$ p$)^{98}$Tc. Our calculations are carried out using the quasi-particle random phase approximation. Numerical results are presented for the energy and temperature dependent cross sections. Since charge exchange reactions by neutrons may also lead to the formation of $^{92}_{41}$Nb and $^{98}_{43}$Tc, we also discuss the feasibility of the ^{92}Mo(n,p)^{92}Nb and ^{98}Ru(n,p)^{98}Tc reactions to produce these nuclei.

PACS numbers: 25.30.Pt, 25.40.Kv, 26.30.-k, 26.30.Jk, 26.50.+x, 97.10.Cv

I. INTRODUCTION

The neutrino (ν) process involves ν-induced reactions on various nuclei during core collapse supernovae (SNe). Large numbers of neutrinos are emitted from a proto-neutron star in the early phase of a SN. Most neutrinos escape from the star, but a small fraction of neutrinos transfer their energy to material in the outer layers of the star by neutrino-nucleus interactions. This process has been proposed as the origin of some rare isotopes of light and heavy elements [1]. The cosmic abundances of these nuclei could thus be valuable tools for studying neutrino spectra from SNe [2, 3], and for constraining neutrino oscillations and/or other ν-physics parameters [4].

Among the many heavy elements, only the two isotopes ^{138}La and ^{180}Ta are currently thought to be synthesized primarily by the ν-process [1, 2]. These two isotopes have similar features: they cannot be produced by either β^+, EC, or β^- decays since in each case stable isobars shield against these decays. Not surprisingly then, the isotopic abundance ratios, ^{138}La/^{139}La and ^{180}Ta/^{181}Ta, are quite small, *i.e.* 0.0902% and 0.012%, respectively [5], making them Nature's rarest isotopes.

In principle, many nuclides are synthesized by the ν-process in SN explosions. The produced abundances, however, are usually negligibly small. This is because the relevant reactions are mediated by a weak interaction compared to production via strong or electromagnetic interactions for the other major nucleosynthesis processes such as the $s-$, $r-$, and $\gamma-$ processes. Thus, the ν-process can only play a dominant role in the synthesis of very rare isotopes that cannot be produced by other means.

Most studies of the ν-process have been concerned with rare stable isotopes such as ^{138}La and ^{180}Ta. In this paper we consider the possibility that some rare unstable nuclei may also be produced via the $\nu-$process. In particular, a recent work [6], has pointed out that the nuclear chart around ^{92}Nb and ^{98}Tc is quite similar to that of ^{138}La and ^{180}Ta as shown in Figs. 1 and 2. These nuclides are shielded from β^+, EC, or β^- decays because of the presence of neighboring stable isobars [7–11]. Therefore, it has been proposed [6] that the two nuclei ^{92}Nb and ^{98}Tc may have a $\nu-$process origin. In this paper we investigate the detailed nuclear physics relevant to this hypothesis.

Although both nuclei are unstable, their half-lives, 3.47×10^7 yr for ^{92}Nb and 4.2×10^6 yr for ^{98}Tc, are long enough to be observed on stellar surfaces or to be incorporated into

meteorites. Indeed, the isotopic abundance ratio of ^{92}Nb/^{93}Nb has been inferred [12, 13] to be $\sim 10^{-3} - 10^{-5}$ at the time of solar system formation. This is comparable to the isotopic ratios for ^{138}La/^{139}La and ^{180}Ta/^{181}Ta. A search for evidence of the extinct unstable isotopes of Tc in meteoritic material has also been made [14], but has not yet been detected. This suggests the abundance of ^{98}Tc at solar-system formation is small compared to the detection limit.

In view of the compelling case for a ν-process origin for ^{92}Nb and ^{98}Tc, this paper explores the nuclear physics relevant to this hypothesis. In Sec. II, we summarize the relevant ν-process reactions. In Sec. III we briefly summarize the QRPA framework used to compute these ν-induced reactions. In Sec. IV, numerical cross sections for neutrino induced reactions on relevant nuclei are given as a function of the incident neutrino energy. Their temperature dependence is also presented for astrophysical applications under the assumption of a Fermi Dirac distribution for the SN neutrinos. A discussion of the roles of charge exchange reactions by neutron capture on nuclei is also given. A summary and conclusions are presented in Sec. V.

II. ν-PROCESS REACTIONS

In the ν-process, a nucleus can be synthesized by either a charged current (CC) or neutral current (NC) reaction. Previous studies have concluded that contributions from the CC reactions are generally larger than those of NC reactions for heavy nuclei [2, 15–17]. The main ν-process reactions for ^{92}Nb are the CC ^{92}Zr$(\nu_e, e^-)^{92}$Nb reaction and the NC ^{93}Nb$(\nu(\bar{\nu}),\ \nu'(\bar{\nu}')$ n $)^{92}$Nb reaction.

Here we note that the dominant reaction for the production of ^{98}Tc is different from that of ^{92}Nb, ^{138}La and ^{180}Tc. For ^{98}Tc, the ^{98}Mo$(\nu_e$,e$^-)^{98}$Tc CC reaction, and the ^{99}Ru$(\nu(\bar{\nu}),\ \nu(\bar{\nu}')\ p)^{98}$Tc NC reaction involving neutrino-induced proton emission to form ^{98}Tc are believed to be the main production mechanisms. Another NC reaction, ^{99}Tc$(\nu(\bar{\nu}),\ \nu'(\bar{\nu}')\ n)^{98}$Tc, might also be possible because ^{99}Mo can easily β decay to ^{99}Tc. However, the half life of ^{98}Tc is 4.2×10^6 yr. This is longer than that of ^{99}Tc, 2.11×10^5 yr, so that ^{98}Tc may be difficult to produce by this NC reaction. The difference between ^{98}Tc and the other three isotopes may imply a different sensitivity to neutrino oscillations and therefore might eventually provide a new probe into the neutrino physics of supernovae.

Moreover, if ^{98}Tc is produced by ν-induced reactions, it might β decay to ^{98}Ru* which subsequently decays by E2 transitions to its ground state with the emission of 0.74536 and 0.65243 MeV γ rays. This situation closely resembles ^{26}Al, whose lifetime is 7.4×10^{7} yr and decays to ^{26}Mg with a 1.809 γ ray (E2 transition) as observed by the COMPTEL detector on the Compton Gamma-Ray Observatory (CGRO) [18].

We presume a two step process in the ν-induced reactions: the 1st step is the formation of excited nuclei by the incident ν's; and the 2nd is the decay process to other ground states via particle emission. To describe the 2nd decay process, one needs to consider the branching ratios for the decay. We estimate these using a Hauser-Feshbach (HF) statistical model [19–23]. One also needs calculations of the transmission coefficients for the emitted particles. In this work, we have made this calculation using the method of Refs. [19, 21].

The nuclear structure of ^{92}Nb and ^{98}Tc are key ingredients for this calculation. For example, excited states with low spins are strongly populated in ^{92}Nb by a Gamow-Teller (GT) transitions from the 0^{+} ground state of the ^{92}Zr parent nucleus. Our scheme for describing such excited states makes use of the standard quasi-particle random phase approximation (QRPA). For the NC reactions, ^{93}Nb(ν, ν')^{93}Nb and ^{99}Ru(ν, ν')^{99}Ru, we generate the ground and excited states of the odd-even target nuclei, ^{93}Nb and ^{99}Ru, by applying quasi-particle operators to the even-even nuclei, ^{92}Zr and ^{98}Ru, which are taken to be the BCS ground state.

III. QRPA FRAMEWORK

The QRPA formalism employed here for the $\nu(\bar{\nu})$-nucleus ($\nu(\bar{\nu})-A$) reactions has been detailed in our previous papers [15–17]. We have applied this formalism to successfully describe the relevant ν-induced reaction data for ^{12}C [15], ^{56}Fe, ^{56}Ni [16], ^{138}La, and ^{180}Ta [17], as well as β, $2\nu2\beta$ and $0\nu2\beta$ decays [24]. In particular, double beta (2β) decay is well known to be sensitive to the nuclear structure and has more data than the ν-induced reaction data. Therefore, it provides a useful constraint for the estimation of ν-process reaction rates.

Charge exchange reactions, A(n,p)B or B(p,n)A, also provide valuable tests of nuclear models. One can deduce the neutrino induced reaction rates from these reactions because, in the low energy regime, Gamow Teller (GT) transitions account for most of the strength in both nucleon exchange and neutrino-induced reactions.

Here we summarize two important characteristics regarding our calculation compared to other QRPA approaches. First, we construct an *ab initio* Brueckner G matrix for the two-body interactions inside nuclei. We do this by solving the Bethe-Salpeter equation based upon the Bonn CD potential for the free-space nucleon-nucleon interaction. This procedure reduces some of the possible ambiguities regarding nucleon-nucleon interactions within nuclei.

Secondly, we include neutron-proton (np) pairing as well as neutron-neutron (nn) and proton-proton (pp) pairing correlations. Consequently, both CC and NC reactions can be described within a single framework.

The contribution from np pairing has been shown to be only of order $1 \sim 2$ % for the weak interactions of light nuclei like ^{12}C, e.g. $\beta^{\pm}$ decay and the $\nu-^{12}$C reaction [15, 16]. Such a small effect in light nuclei is easily understood because the energy gaps between the neutron and proton energy spaces are too large to be effective. However, in intermediate-mass nuclei, such as ^{56}Fe and ^{56}Ni, the np pairing effect accounts for $20 \sim 30$ % of the total cross section [16]. Therefore, for the heavy nuclei of interest in the present work, np pairing should be taken into account.

The np pairing has two isospin contributions, T = 1 and T = 0. These correspond to J = 0 and J = 1 pairings, respectively. Since the J = 0 (T = 1) pairing couples a state to its time reversed state, the shape is almost spherical. Hence, the J = 0 (T = 1) np pairing can be easily included in our spherically symmetric model.

The J = 1 (T = 0) np pairing, however, is partially associated with a tensor force. This leads to a non-spherical shape, *i.e.* deformation. Therefore, in principle, the J = 1 (T = 0) np coupling cannot be included in a spherically symmetrically model. However, if we use a re-normalized strength constant for the np pairing, g_{np}, as a parameter to be fitted to the empirical np pairing gap, the J = 1 (T = 0) pairing can be incorporated implicitly even in a spherically symmetric model. This is because the fitted g_{np} effectively includes the effects of nuclear deformation.

The empirical np pairing gap, $\delta_{pn}^{emp.}$, is easily extracted from data on mass-excesses. Hence, we can compare these to the theoretical pairing gap, $\delta_{np}^{th.}$, calculated from the difference between the total energies with and without np pairing correlations [24]

$$\delta_{pn}^{emp.} = \pm\frac{1}{4}\{2[M(Z,N+1)+M(Z,N-1)+M(Z-1,N)+M(Z+1,N)] \qquad (1)$$

$$
\begin{aligned}
& -[M(Z+1,N+1)+M(Z-1,N+1)+M(Z-1,N-1)+ \\
& M(Z+1,N-1)]-4M(Z,N)\} \ , \\
\delta_{np}^{th.} \ &= \ -[(H_0^{'}+E_1^{'}+E_2^{'})-(H_0+E_1+E_2)] \ ,
\end{aligned}
$$

where $H_0^{'}(H_0)$ is the Hartree-Fock energy of the ground state with (without) np pairing and $E_1^{'}+E_2^{'}$ (or E_1+E_2) is the sum of the lowest two quasi-particles energies with (without) np pairing correlations. More detailed discussion of this is given in Ref. [24].

Our calculation starts from the following Hamiltonian

$$
H = H_0 + H_{int} \ , \tag{2}
$$

where

$$
H_0 = \sum_{a^{'}\alpha} \epsilon_{a\alpha} c_{a\alpha}^{+} c_{a\alpha} \ , \tag{3}
$$

and

$$
H_{int} = \sum_{a^{'}b^{'}c^{'}d^{'},\alpha\beta\gamma\delta} V_{a\alpha b\beta c\gamma d\delta} c_{a\alpha}^{+} c_{b\beta}^{+} c_{d\delta} c_{c\gamma} \ . \tag{4}
$$

Here, the interaction matrix V is the anti-symmetrized interaction of the Baranger Hamiltonian. It has two factors of $-1/2$ from J and T couplings, so that the H_{int} in Eq.(2) is equivalent to the usual $H_{int} = \frac{1}{4}\Sigma_{a^{'}b^{'}c^{'}d^{'},\alpha\beta\gamma\delta}\tilde{V}_{a\alpha b\beta c\gamma d\delta} c_{a\alpha}^{+} c_{b\beta}^{+} c_{d\delta} c_{c\gamma}$. Roman letters indicate quantum numbers of nucleon states if total angular momentum j_a, *i.e.* $a = (n_a, l_a, j_a)$, while primed Roman letters also include the magnetic sub-states, *i.e.* $a^{'} = (n_a, l_a, j_a, m_a)$. The isospin of real particles is denoted as a Greek letter while the isospin of quasi-particles is expressed as a primed Greek letter. The operators $c_{a\alpha}^{+}$ and $c_{a\alpha}$ stand for the usual creation and destruction operators for nucleons in a state $a^{'}$ with isospin α, while $c_{\bar{d}\delta} = c_{n_d,l_d,j_d,-m_d}(-)^{j_d-m_d}$ is the time reversed operator of $c_{d\delta}$.

We use the general Hartree-Fock-Bogoliubov (HFB) transformation to rewrite this Hamiltonian in a quasi-particle basis,

$$
a_{c\mu^{'}}^{+} = \sum_{d^{'}\delta} (u_{c^{'}\mu^{'}d^{'}\delta} c_{d\delta}^{+} + v_{c^{'}\mu^{'}d^{'}\delta} c_{\bar{d}\delta}) \ , \ a_{\bar{c}\mu^{'}} = \sum_{d^{'}\delta} (u_{\bar{c}^{'}\mu^{'}\bar{d}^{'}\delta}^{*} c_{\bar{d}\delta} + v_{\bar{c}^{'}\mu^{'}\bar{d}^{'}\delta}^{*} c_{d\delta}^{+}) \ . \tag{5}
$$

Here, time reversal invariance and spherical symmetry are presumed. Hence, we do not mix single particle states of different angular momenta. The Hamiltonian can then be represented in terms of quasi-particles as follows

$$
H^{'} = H_0^{'} + \sum_{a^{'}\alpha^{'}} E_{a\alpha^{'}} a_{a\alpha^{'}}^{+} a_{a\alpha^{'}} + H_{qp.int} \ . \tag{6}
$$

Applying the BCS transformation to Eq.(3) we obtain the following HFB equation

$$\begin{pmatrix} \epsilon_p - \lambda_p & 0 & \Delta_{p\bar{p}} & \Delta_{p\bar{n}} \\ 0 & \epsilon_n - \lambda_n & \Delta_{n\bar{p}} & \Delta_{n\bar{n}} \\ \Delta_{p\bar{p}} & \Delta_{p\bar{n}} & -\epsilon_p + \lambda_p & 0 \\ \Delta_{n\bar{p}} & \Delta_{n\bar{n}} & 0 & -\epsilon_n + \lambda_n \end{pmatrix}_c \begin{pmatrix} u_{\alpha' p} \\ u_{\alpha' n} \\ v_{\alpha' p} \\ v_{\alpha' n} \end{pmatrix}_c = E_{c\alpha'} \begin{pmatrix} u_{\alpha' p} \\ u_{\alpha' n} \\ v_{\alpha' p} \\ v_{\alpha' n} \end{pmatrix}_c , \quad (7)$$

where $E_{c\alpha'}$ is the energy of a quasi particle with isospin quantum number α' in the state c. Pairing potentials Δ_p, Δ_n and Δ_{pn} in Eq.(7) are adjusted to reproduce the empirical paring gaps. This is achieved by multiplying by strength parameters, g_p, g_n, g_{np} that arise from the renormalization of the finite particle model space [24]. Detailed parameters for each nucleus are given in Sec. IV. If we neglect Δ_{np}, this equation reduces to the standard BCS equation.

In our QRPA calculation, the ground state of the target nucleus is described by a BCS vacuum for quasi-particles which undergo nn, pp and np pairing correlations. Excited states, $|m; J^\pi M\rangle$, in the compound nucleus are generated by operating the following one phonon operator on the correlated QRPA vacuum

$$Q^{+,m}_{JM} = \sum_{kl\mu'\nu'} [X^m_{(k\mu' l\nu' J)} C^+(k\mu' l\nu' JM) - Y^m_{(k\mu' l\nu' J)} \tilde{C}(k\mu' l\nu' JM)] , \quad (8)$$

where the pair creation and annihilation operators, C^+ and $\tilde{C}$, are defined by

$$C^+(k\mu' l\nu' JM) = \sum_{m_k m_l} C^{JM}_{j_k m_k j_l m_l} a^+_{l\nu'} a^+_{k\mu'} , \; \tilde{C}(k\mu' l\nu' JM) = (-)^{J-M} C(k\mu' l\nu' J - M) , \quad (9)$$

where $a^+_{l\nu'}$ is the quasi-particle creation operator, and the $C^{JM}_{j_k m_k j_l m_l}$ are Clebsch-Gordan coefficients. Here, Roman letters indicate single particle states, while primed Greek letters denote quasi-particles of type 1 or 2.

If neutron-proton pairing is neglected, the quasi-particles become quasi-protons and quasi-neutrons, and the phonon operator is easily decoupled into two different operators: One is for charge changing reactions such as nuclear β decay and CC neutrino reactions; The other is for charge conserving reactions such as electromagnetic and NC neutrino reactions. We denote the forward and backward going amplitudes from the ground states to excited states by $X_{a\alpha',b\beta'}$ and $Y_{a\alpha',b\beta'}$. These are obtained from the QRPA equation.

A detailed derivation of the QRPA was given in Refs. [16, 24]. The particle-particle strength parameters, g_{pp}, are adjusted to the Gamow Teller Giant Resonance (GTGR) states and the particle-particle strength parameters, g_{ph}, are taken as 1.0 in this calculation. The

spurious states in the QRPA are avoided by discarding the imaginary solutions to the QRPA equation and the particle non-conservation problem peculiar to the QRPA approach is properly treated by requiring that the averaged particle number be a real particle number.

By using the phonon operator $Q^{+,m}_{JM}$ in Eq.(8), we obtain the following expression for the CC neutrino reactions

$$\begin{aligned} & \langle QRPA||\hat{\mathcal{O}}_\lambda||\ \omega; JM\rangle \\ = & \sum_{a\alpha' b\beta'} [\mathcal{N}_{a\alpha' b\beta'} \langle a\alpha'||\hat{\mathcal{O}}_\lambda||b\beta'\rangle\ [u_{pa\alpha'} v_{nb\beta'} X_{a\alpha' b\beta'} + v_{pa\alpha'} u_{nb\beta'} Y_{a\alpha' b\beta'}]\ , \end{aligned} \tag{10}$$

where $\mathcal{N}_{a\alpha' b\beta'}(J) \equiv \sqrt{1-\delta_{ab}\delta_{\alpha'\beta'}(-1)^{J+T}}/(1+\delta_{ab}\delta_{\alpha'\beta'})$. This form easily reduces to the result usually used in the proton-neutron QRPA (pnQRPA) when the np pairing correlations are removed [35]

$$\langle QRPA||\hat{\mathcal{O}}_\lambda||\ \omega; JM\rangle = \sum_{apbn} [\mathcal{N}_{apbn} \langle ap||\hat{\mathcal{O}}_\lambda||bn\rangle\ [u_{pa} v_{nb} X_{apbn} + v_{pa} u_{nb} Y_{apbn}]\ . \tag{11}$$

Since the NC reactions for ^{93}Nb and ^{99}Ru occur in odd-even nuclei, we need to properly describe the ground state of odd-even nuclei. The standard QRPA treats the ground state of even-even nuclei as a BCS vacuum, so it is not easily applicable to reactions on odd-even nuclei.

Our formalism to deal with such NC reactions is based upon the quasi-particle shell model (QSM) [17, 25]. First, we generate low energy spectra of odd-even nuclei by applying a one quasi-particle creation operator to the even-even BCS ground state, *i.e.* $|\Psi_i\rangle = a^+_{i\mu'}|BCS\rangle$ and $|\Psi_f\rangle = a^+_{f\nu'}|BCS\rangle$.

It is well known that 3 quasi-particle excited states may appear as the high spin states in odd-even nuclei [26–28]. In this work, however, we take only the yrast states into account by assuming that the high spin states of ^{93}Nb [29, 30] and ^{99}Ru generated beyond the 1 quasi-particle structure quickly decay into an yrast state prior to particle emission. This is justified because the maximum particle emission transition rates for odd-even nuclei turn out to come from a cascade of transitions through the yrast states to the ground state [21].

However, sometimes an yrast state generated by a 3 quasi-particle configuration can even become the ground state of an odd nucleus [31, 32]. Hence, 1 quasi-particle states alone may be not sufficient to properly describe the excited states relevant to the neutrino induced reactions on the odd-even nuclei considered here. Recent calculations including 3 quasi-particle states (Ref. [32]) might be a useful approach for NC reactions on odd-even

nuclei, however, that complexity is beyond the scope of the present work. Since we neglect the 3 quasi-particle states here, however, our results for the NC reactions on odd-odd nuclei should be regarded as a lower limit to the possible cross section for NC neutrino reactions.

The NC weak transitions are given by

$$\begin{aligned} & \sum_{i\mu' f\nu'} \langle J_f||\hat{\mathcal{O}}_\lambda||J_i\rangle \qquad (12) \\ = & \sum_{\mu' f\nu'} [\langle fp||\hat{\mathcal{O}}_\lambda||ip\rangle \; u_{fp\nu'}u_{ip\mu'} + (-)^{j_a+j_b+\lambda}\langle ip||\hat{\mathcal{O}}_\lambda||fp\rangle \; v_{ip\mu'}v_{fp\nu'}] + (p \to n) \; . \end{aligned}$$

The weak current operator is comprised of longitudinal, Coulomb, electric and magnetic operators, $\hat{O}_\lambda$, as described in Ref. [16]. Finally, with the initial and final nuclear states specified, the cross sections for $\nu(\bar{\nu}) - A$ reactions via the weak transition operator can be directly calculated from the formulas of Refs. [33, 34]. For CC reactions we multiplied by the Cabibbo angle $cos^2\theta_c$ and took account of the Coulomb distortion of the outgoing leptons [19, 35].

IV. RESULTS AND DISCUSSIONS

A. GT strength functions

Figure 3 shows the GT(−) strength distributions and the running sum for ^{92}Zr. Results are shown for both the pnQRPA (left) and the QRPA (right) models. Here the pnQRPA model considers only nn and pp pairing correlations, while the QRPA also includes np pairing in addition. The np pairing redistributes the GT(–) strength obtained from the pnQRPA. The experimental GT(–) data are only known for the low-lying states below 7 MeV. These were extracted from the ^{92}Zr$(p,n)^{92}$Nb reaction at E_p = 25 MeV [36]. The running sum measured up to 6.28 MeV w.r.t. ^{92}Nb is 2.3. This agrees well with our results shown in Fig.3, i.e. 2.5 (pnQRPA) and 2.7 (QRPA).

The difference between the pnQRPA and QRPA model results appears in the strength around 11 (9) MeV w.r.t. the ^{92}Zr (^{92}Nb) ground state. This figure shows that one could determine which is the better description by measuring charge exchange reactions on ^{92}Zr with energies higher than 25 MeV [36]. We take g_p, g_n, g_{np} to be 1.064(1.025), 1.015(1.059) and 1.932(1.967) for ^{92}Zr (^{98}Mo) to fit the empirical pairing gaps. For the particle model space, 10 (11) single particle states from the ^{40}Ca core are taken into account for ^{92}Zr (^{98}Mo).

These GT strengths are important for understanding the ν-process origin of the proton-rich (neutron-deficient) nucleus, ^{92}Nb. Here we show results for ν-induced reactions for ^{92}Nb and ^{98}Tc. Detailed formulae for the cross sections were presented in our previous papers [16, 17]. For CC reactions, we consider the Coulomb distortion of the outgoing lepton. Since the neutrino energies of interest here can go up to 80 MeV, we divide the energy range into two regions. In the low energy region, we use the Fermi correction used for the s-wave electron in β decay. In the high energy region, however, we exploit the effective momentum approach (EMA) used for intermediate energy electron scattering analysis [37–39]. To make a smooth transition of the cross sections between the two energy limits, we determine an energy point, henceforth referred to as the Coulomb cut. Below this cut we use the Fermi correction while above the cut the EMA is used. We show results for two different Coulomb cuts, 30 and 40 MeV. Although, in the case of a 30 MeV Coulomb cut the cross sections change more smoothly with energy, the temperature dependent cross sections turn out to be nearly independent of the location of the Coulomb cut. Of course, the Coulomb cut could be lower for lighter nuclei, such as ^{12}C [15] and ^{40}Ar [40].

B. Averaged cross sections

Incident $\nu(\bar{\nu})$ energies emitted in SN explosions [1, 4] are expected to be in the energy range of a few MeV to tens of MeV because the $\nu(\bar{\nu})$ energy spectra emitted from the proto-neutron star approximately follow a Fermi-Dirac distribution given by a temperature T and a chemical potential α [4, 41]. Therefore, the averaged temperature-dependent cross sections can be deduced from an integral over a Fermi-Dirac ν-distribution,

$$\langle \sigma_\nu \rangle = \frac{1}{N} \int dE_\nu \sigma_\nu(E_\nu) f(E_\nu) Br \ , \ f(E_\nu) = \frac{E_\nu^2}{exp[(E_\nu/T) - \alpha] + 1} \ , \tag{13}$$

where $\sigma_\nu(E_\nu)$, $f(E_\nu)$ and Br are the energy dependent $\nu - A$ cross sections, the corresponding neutrino flux and the branching ratios of the excited states, respectively. N is a normalization factor given by $\int dE_\nu f(E_\nu) Br$. To study the nucleosynthesis [19] or ν-oscillations [4] during a SN explosion, one must specify a realistic temperature and chemical potential for each neutrino species. For our purposes, we adopt $T = 3.2,\ 5.0$ and 6.0 MeV for $\nu_e, \bar{\nu}_e$ and $\nu_{\mu,\tau}(\bar{\nu}_{\mu,\tau})$, respectively, and we set $\alpha = 0$ [4, 19].

To deduce the final nuclear abundances of ^{92}Nb and ^{98}Tc, it is necessary to multiply the

temperature dependent cross sections from the relevant compound nuclei by the particle emission branching ratios, Br, to the ^{92}Nb or ^{98}Tc ground state. These are obtained from Hauser-Feshbach theory [20], using the JENDL3-3 model and the calculated transmission coefficients of Ref. [21].

C. Results for ^{98}Tc

The upper panels in Figure 4 show the energy dependence of the cross sections for CC reactions relevant to ^{98}Tc production, *i.e.* $^{98}\mathrm{Mo}(\nu_e, e^-)^{98}\mathrm{Tc}$. The lower panels show the temperature-dependent thermally averaged cross sections. The left column is for a 40 MeV Coulomb cut, while the right column shows results for a 30 MeV cut. The cross sections as a function of energy are slightly smoother for the 30 MeV Coulomb cut [35]. Hence, it seems to be preferred over the 40 MeV case. Nevertheless, the thermally averaged cross sections (lower panels) are nearly independent of the cut. Our energy-dependent cross sections exhibit typical behavior for CC cross sections for even-even nuclei. Namely, GT 1^+ and Fermi 0^+ transitions dominate the total cross section below 40 MeV, however, the contributions from higher multipole transitions, such as the spin dipole resonance, increase above 40 MeV.

The red curves in the lower panels show the temperature dependent cross sections for the CC reaction. It is clear from a comparison of the left and right lower panels that different Coulomb cuts do not affect the thermally averaged cross sections. Blue and green curves show cross sections multiplied by the branching ratios for proton and neutron emission from the ^{98}Tc* excited nucleus. Since the neutron separation energy of ^{98}Tc, $S_n = 7.279$ MeV, is larger than the proton separation energy, $S_p = 6.176$ MeV, proton emission is much easier than neutron decay. Hence, the cross sections for proton emission are larger than those for neutron decay. Of course, these two decays have no bearing on the formation of ^{98}Tc.

Figure 5 shows the energy dependent cross sections for the $^{99}\mathrm{Ru}(\nu(\bar{\nu}), \nu'(\bar{\nu}'))^{99}\mathrm{Ru}$ NC reactions. The upper two figures are for incident ν_μ (left) and ν_e (right). The lower two figures are for the anti-neutrinos, *i.e.* $\bar{\nu}_\mu$ (left) and $\bar{\nu}_e$ (right). Note that the cross sections for ν_e and ν_μ are almost identical. There is, however, a difference in scale between the upper (neutrino) and lower (anti-neutrino) panels. Therefore, although NC reactions are nearly independent of neutrino species, they do depend upon the helicity of the incident neutrinos.

It is also an interesting point that the cross sections for incident ν's are larger than those for incident $\bar{\nu}$'s even in the case of the NC reactions [40]. All cross sections below 40 MeV are dominated by the GT 1^+ transition, which is typical of NC reactions.

Figure 6 shows the temperature dependent cross sections corresponding to Fig. 5. The upper two curves are for ν_μ (left) and ν_e (right), while the lower figures show cross sections for $\bar{\nu}_\mu$ (left) and $\bar{\nu}_e$ (right). Here we have only shown results for a Coulomb cut = 40 MeV because the thermally averaged cross sections are nearly independent of the cuts as shown in Fig. 4. The red curves are for the case of no particle emission, while the blue and green curves include branching ratios for neutron and proton emission *i.e.* $^{99}\mathrm{Ru}(\nu(\bar{\nu}), \nu^{'}(\bar{\nu}^{'})\ n)^{98}\mathrm{Ru}$ and $^{99}\mathrm{Ru}(\nu(\bar{\nu}), \nu^{'}(\bar{\nu}^{'})\ p)^{98}\mathrm{Tc}$, respectively. Similarly to the energy dependent cross sections, they are independent of the neutrino species, but depend upon neutrino helicities as can be seen in Fig. 6. These results demonstrate that, in contrast to the results for CC reactions, the cross sections for proton emission are smaller than those for neutron emission. This is because in this case the neutron separation energy (S_n = 7.464 MeV) is less than that for protons (S_p = 8.478 MeV) for ^{99}Ru.

The green curves for the $^{99}\mathrm{Ru}(\nu(\bar{\nu}), \nu^{'}(\bar{\nu}^{'})\ p)^{98}\mathrm{Tc}$ reactions can help to clarify the physical environment for the formation of ^{98}Tc. The temperature dependence of this reaction could play a role in understanding both the neutrino temperatures in the $\nu-$process environment and possible effects from neutrino oscillations. Once formed, ^{98}Tc may β decay to ^{98}Ru with a half life of 4.2×10^6 yr. The β decay to excited states in ^{98}Ru would be accompanied by E2 transitions to the ground state with γ ray energies of 0.74536 MeV and 0.65243 MeV. Such transitions may be observable via gamma-ray astronomy as in the case of ^{26}Al in the Galaxy.

D. Results for ^{92}Nb

The abundance of ^{92}Nb and its isotopic ratio $^{92}\mathrm{Nb}/^{93}\mathrm{Nb}$ are of astrophysical interest because ^{92}Nb is hypothesized [6] to have been produced by the ν-process and the $^{92}\mathrm{Nb}/^{93}\mathrm{Nb}$ ratio may be useful as a chronometer of the early solar system [6, 7].

The upper panels in Fig.7 show the energy dependent cross sections for the CC $^{92}\mathrm{Zr}(\nu_e, e^-)^{92}\mathrm{Nb}$ reaction. As in the case of the CC reaction to produce ^{98}Tc, the 30 MeV Coulomb cut is slightly preferred, but the location of the cut does not significantly affect

the thermally averaged cross sections as shown in the lower panels. Since the neutron separation energy of ^{92}Nb (S_n = 7.883 MeV) is larger than the proton separation energy (S_p = 5.846 MeV), proton emission is much easier than neutron emission. This leads to a larger proton-emission cross section than that of neutron decay. This is also similar to the case of ^{98}Tc.

All of the results for the ν-induced reactions on ^{92}Nb resemble those for ^{98}Tc. In particular there is a similar energy and temperature dependence of the cross sections. As is the case of ^{98}Tc the red curves in the lower panels may be useful for understanding the temperature conditions in the astrophysical site producing ^{92}Nb. The results for ^{92}Nb production via NC neutrino induced reactions are presented in Fig. 8. Only results for the ν_e and $\bar{\nu}_e$ are given because they are almost identical to those for the ν_μ and $\bar{\nu}_\mu$ reactions.

The general trends in the energy and temperature dependent cross sections by NC reactions on ^{93}Nb are shown in Fig. 9. They have no special characteristics compared to the results for ^{99}Ru in Fig. 6 except that the cross section for proton emission is larger than that for neutron emission because in this case the neutron separation energy (S_n = 8.831 MeV) is larger than that for protons (S_p = 6.043 MeV0 in ^{93}Nb. The magnitudes of the cross sections are about 1.5 times smaller than those for ^{99}Ru. Finally, in Table 1, we summarize the averaged cross sections for typical [42] average neutrino energies and temperature to be used in nucleosynthesis calculations.

E. Charge exchange reactions for ^{98}Tc and ^{92}Nb

We note here that the 15 $M_\odot$ progenitor model of Heger and Woosley [43] shows significant ^{92}Nb yield before the arrival of the supernova shock. This arises from the charge exchange reaction ^{92}Mo(n,p)^{92}Nb during core carbon burning [44]. However, their network calculation does not take account of the (n, γ) destruction of ^{92}Nb. Therefore, one should consider the feasibility of the formation of ^{98}Tc and ^{92}Nb nuclei by (n,p) reactions in an environment that includes the (n, γ) destruction of ^{92}Nb.

To explore this consider the ^{98}Ru(n,p)^{98}Tc and ^{92}Mo(n,p)^{92}Nb production reactions in a core helium burning s-process that occurs during the pre-supernova evolution. The Q value for the ^{98}Ru(n,p)^{98}Tc reaction is negative Q_{np} = – 1.014 MeV, so that even neutrons with energies around a few hundred keV cannot capture to produce ^{98}Tc. However, the

TABLE I: Averaged cross sections in units of $10^{-42}cm^2$ for ^{98}Mo via CC and ^{99}Ru via NC, and ^{92}Zr via CC and ^{93}Nb via NC with the particle emission. Neutrino temperatures are taken from [4] and $\langle E_k \rangle$ is calculated from the $\langle E_k \rangle / T \sim 3.1514 + 0.1250\alpha$ with $\alpha = 0$ [31, 42].

Reactions	$\langle E_k \rangle$ [MeV]	T [MeV]	$\langle \sigma \rangle$
$^{98}\mathrm{Mo}(\nu_e, e^-)^{98}\mathrm{Tc}$	10.08	3.2	7.77
$^{98}\mathrm{Mo}(\nu_e, e^- p)^{97}\mathrm{Mo}$	10.08	3.2	1.90
$^{98}\mathrm{Mo}(\nu_e, e^- n)^{97}\mathrm{Tc}$	10.08	3.2	0.09
$^{99}\mathrm{Ru}(\bar{\nu}_\mu, \bar{\nu}'_\mu)^{99}\mathrm{Ru}$	18.90	6.0	78.5
$^{99}\mathrm{Ru}(\bar{\nu}_\mu, \bar{\nu}'_\mu n)^{98}\mathrm{Ru}$	18.90	6.0	14.6
$^{99}\mathrm{Ru}(\bar{\nu}_\mu, \bar{\nu}'_\mu p)^{98}\mathrm{Tc}$	18.90	6.0	1.70
$^{99}\mathrm{Ru}(\bar{\nu}_e, \bar{\nu}'_e)^{99}\mathrm{Ru}$	15.75	5.0	52.1
$^{99}\mathrm{Ru}(\bar{\nu}_e, \bar{\nu}'_e n)^{98}\mathrm{Ru}$	15.75	5.0	10.5
$^{99}\mathrm{Ru}(\bar{\nu}_e, \bar{\nu}'_e p)^{98}\mathrm{Tc}$	15.75	5.0	0.92
$^{92}\mathrm{Zr}(\nu_e, e^-)^{92}\mathrm{Nb}$	10.08	3.2	8.92
$^{92}\mathrm{Zr}(\nu_e, e^- p)^{91}\mathrm{Zr}$	10.08	3.2	2.32
$^{92}\mathrm{Zr}(\nu_e, e^- n)^{91}\mathrm{Nb}$	10.08	3.2	0.42
$^{93}\mathrm{Nb}(\bar{\nu}_\mu, \bar{\nu}'_\mu)^{93}\mathrm{Nb}$	18.90	6.0	46.8
$^{93}\mathrm{Nb}(\bar{\nu}_\mu, \bar{\nu}'_\mu n)^{92}\mathrm{Zr}$	18.90	6.0	1.04
$^{93}\mathrm{Nb}(\bar{\nu}_\mu, \bar{\nu}'_\mu p)^{92}\mathrm{Nb}$	18.90	6.0	4.90
$^{93}\mathrm{Nb}(\bar{\nu}_e, \bar{\nu}'_e)^{93}\mathrm{Nb}$	15.75	5.0	30.0
$^{93}\mathrm{Nb}(\bar{\nu}_e, \bar{\nu}'_e n)^{92}\mathrm{Zr}$	15.75	5.0	0.60
$^{93}\mathrm{Nb}(\bar{\nu}_e, \bar{\nu}'_e p)^{92}\mathrm{Nb}$	15.75	5.0	3.92

^{92}Mo(n,p)^{92}Nb reaction has a Q value of $Q_{np} = 0.42671$ MeV, and hence, may occur for typical s-process neutron energies of $kT \sim 30$ – 100 keV.

The spin and parity for states below ~ 0.5 MeV in ^{92}Nb are $J^\pi = 7^+(0.0)$, $2^+(0.135)$, $2^-(0.225)$, $3^+(0.285)$, $5^+(0.353)$, $3^-(0.390)$, $4^+(0.480)$ and $6^+(0.501)$. The two lowest states of the ^{92}Nb + p system have $J^\pi = \frac{15}{2}^+$ or $\frac{13}{2}^+$ for the ground state and $J^\pi = \frac{5}{2}^+$ or $\frac{3}{2}^+$ for the 1st excited state.

Since the configuration of the entrance-channel ^{92}Mo+n system can be represented as

$0^+ \otimes \frac{1}{2}^+ \otimes l_n^\pi$, we need at least d-wave incident neutrons (*i.e.* $l_n^\pi \geq 2^+$) to form a $\frac{5}{2}^+$ or $\frac{3}{2}^+$ state in the ^{93}Mo compound nucleus. Even if we consider the excited states of ^{92}Nb below $\sim$ 0.5 MeV, which would only be slightly populated at a typical s-process temperature of kT $\sim$ 30 keV, only the 2^- (0.225 MeV) and 3^- (0.389 MeV) states are allowed. Due to the conservation of angular momentum, however, populating these states requires exit-channel protons with at least $l_p^\pi = 1^-$.

There is no experimental data for the ^{92}Mo(n,p)^{92}Nb reaction below 1.5 MeV. However, according to theoretical calculations by ENDF/B-VII.0 [45] the reaction cross section to individual states is typically smaller than 0.1 μb for neutrons at energies below 1 MeV and the thermally averaged cross sections for 30 keV neutrons might be much smaller than 0.1 μb. To check this we carried out a HF statistical model calculation at the threshold energy using the JENDL-4 data [46]. The calculated Maxwellian-averaged cross sections for ^{92}Mo(n,p)^{92}Nb turns out to be extremely small $\langle \sigma v \rangle / v_T = 4.02 \times 10^{-13} \mu b$ and $5.39 \times 10^{-4} \mu b$ at neutron energies of 30 keV and 100 keV, respectively, where $\langle\ \rangle$ denotes the Maxwellian average, σ is the cross section, v is the relative velocity between incident neutrons and the target nucleus, and v_T is the mean thermal velocity.

Once ^{92}Nb is produced by the (n,p) reaction on ^{92}Mo, it remains exposed to the same intense flux of neutrons and is destroyed by radiative neutron capture reactions via ^{92}Nb(n,γ)^{93}Nb. Although the (n,γ) cross section has not been measured for the radioactive nucleus ^{92}Nb ($\tau_{1/2} = 3.47 \times 10^7 y$), the ^{92}Nb(n,$\gamma$)^{93}Nb cross section is expected to be comparable to those measured for stable Nb isotopes, $\langle \sigma v \rangle / v_T$ = 261.3, 317.2, and 402.6 mb for ^{93,94,95}Nb(n,γ)^{94,95,96}Nb reactions, respectively, at a neutron energy 30 keV [21]. These (n,γ) cross sections are eighteen orders of magnitude larger than the ^{92}Mo(n,p)^{92}Nb cross section at this energy. Therefore, the ^{92}Mo(n,p)^{92}Nb reaction should not contribute much to the production of ^{92}Nb in the weak s-process during the core helium burning phase of pre-supernova massive stars.

V. SUMMARY

We have applied the Quasi-particle RPA method to calculate neutrino-induced reaction rates for the two odd-odd nuclei ^{98}Tc and ^{92}Nb. These nuclei are of interest because they may be produced by the ν-process in core-collapse supernovae. The abundance of ^{98}Tc may

eventually be measurable by observing the γ-rays from the E2 transition to the ground state of the daughter nucleus ^{98}Ru. If so, it may play a role as a γ-ray probe of the operation of the ν-process similar to the role of ^{26}Al gamma rays as a probe of hot hydrogen burning in the Galaxy.

Similarly, the ^{92}Nb/^{93}Nb abundance ratio could help to constrain neutrino properties in ν-process nucleosynthesis as in the case of ^{138}La and ^{180}Ta whose isotopic abundances place valuable physical constraints on the the average ν-process neutrino temperature [5].

The energy and temperature dependent cross sections for the CC ^{92}Nb, ^{92}Zr$(\nu_e, e^-)^{92}$Nb and NC ^{93}Nb$(\nu,\ \nu^{'}$ n $)^{92}$Nb reactions are presented. For ^{98}Tc, the ^{98}Mo$(\nu_e, e^-)^{98}$Tc CC reaction and the ^{99}Ru$(\nu,\ \nu^{'}$ p$)^{98}$Tc NC reaction have been estimated using the QRPA. Particle emission from the compound nuclei produced by the ν-process make use of branching ratios based upon theoretical transmission coefficients calculated in a Hauser-Feshbach statistical model.

Deduced cross sections for these nuclei show features typical of NC and CC neutrino induced reactions. The calculated CC reactions are dominated by GT transitions below 40 MeV, but other multipole transitions become important at higher energy. In the case of the NC reactions, the GT dominance becomes more significant in the low energy region. One more point of note regarding the NC reactions is that they are nearly independent of neutrino species, but instead depend upon the neutrino helicity.

For the NC neutrino reactions on odd-even nuclei we have made the assumption that excited states beyond a 1 quasi-particle configuration quickly decay to the yrast states before particle emission. This assumption may be inadequate for the yrast states stemming from 3 quasi-particle admixtures. Such 3 quasi-particle states may contribute to the cross section of the NC neutrino reaction. In that sense the NC cross sections for odd nuclei presented here should be considered as lower limits. In a future work we will consider a more advanced approach that takes into account excited states beyond the 1 quasi-particle level.

Finally, we have considered the possibility that (n,p) reactions might also produce these nuclei. Although he ^{98}Ru(n,p)^{98}Tc reaction cannot contribute because of its negative Q_{np} value, the ^{92}Mo(n,p)^{92}Nb charge exchange reaction by thermal neutrons might affect the initial abundance ratio of ^{92}Nb/^{93}Nb before the supernova explosion. However, the (n,p) reaction is not expected to be an significant contributer to the production of pre-solar ^{92}Nb because the ^{92}Nb(n,γ)^{93}Nb destruction reaction cross section is $\sim 10^{18}$ times larger than

that of ^{92}Mo(n,p)^{92}Nb production reaction for neutrons of the energy $\sim$ 30 keV. Therefore, any produced ^{92}Nb is expected to be quickly destroyed. Nevertheless, more detailed calculations of the production and destruction of ^{92}Nb before and during the ν-process are clearly desired. Indeed, calculations of ^{92}Nb and ^{98}Tc nucleosynthesis in SN explosions are currently underway and will be reported in a separate paper [6]. These calculations will consider the neutrino reactions described here along with more realistic calculations of the charge exchange reactions.

Acknowledgments

This work was supported by the National Research Foundation of Korea (2011-0015467, 2011-0003188) and one of authors (Cheoun) was supported by the Soongsil University Research Fund. This work was also supported in part by Grants-in-Aid for Scientific Research of JSPS (20244035), and in part by U.S. Department of Energy under Nuclear Theory Grant DE-FG02-95-ER40934, and in part by Grants-in-Aid for JSPS Fellows (21.6817).

[1] S. E. Woosley, D. H. Hartmann, R. D. Hoffman, and W. C. Haxton, Astrophys. J. **356**, 272 (1990).

[2] A. Heger, E. Kolbe, W. C. Haxton, K. Langanke, G. Martínez-Pinedo, S. E. Woosley, Phys. Lett. **B 606**, 258 (2005).

[3] T. Yoshida, T. Kajino, D-H. Hartmann, Phys. Rev. Lett. **94**, 231101 (2005).

[4] T. Yoshida, T. Kajino, H. Yokomakura, K. Kimura, A. Takamura, D-H. Hartmann, Astrophys. J. **649**, 319 (2006).

[5] T. Hayakawa, T. Kajino, S. Chiba, G. J. Mathews, Phys. Rev. C **81**, 052801(R) (2010).

[6] T. Hayakawa, K. Nakamura, T. Kajino, S. Chiba, N. Iwamoto, M. K. Cheoun, G. J. Mathews, submitted for publication, (2012).

[7] Q. Z. Yin, *et al.*, Astrophys. J. **536**, L49-L53 (2000).

[8] D. D. Clayton, *et al.*, Astrophys. J. **214**, 300-315 (1977).

[9] C. Münker, *et al.*, Science, **289**, 1538-1542 (2000).

[10] Q. Z. Yin, S. B. Jacobsen, Meteoritics and Planetary Science **69**, 5208 (2002).

[11] B. S. Meyer, Nucl. Phys. **A 719**, 13-20 (2003).

[12] M. Schönbächler, *et al.*, Science **295**, 1705-1708 (2002).

[13] M. Schönbächler, *et al.*, Geochimica at Cosmochimica Acta **69**, 775-785 (2005).

[14] N. Dauphas, B. Marty, and L. Reisberg, Astrophys. J. **565**, 640 (2002).

[15] Myung-Ki Cheoun, Eunja Ha, S. Y. Lee, K. S. Kim, W. Y. So, and T. Kajino, Phys. Rev. **C 81**, 028501 (2010).

[16] Myung-Ki Cheoun, Eunja Ha, K. S. Kim and T. Kajino, J. of Phys. **G 37**, 055101 (2010).

[17] Myung-Ki Cheoun, Eunja Ha, T. Hayakawa, T. Kajino, S. Chiba, Phys. Rev. **C 82**, 035504 (2010).

[18] http:/heasarc.gsfc.nasa.gov/docs/cgro/index.html

[19] T. Suzuki, S. Chiba, T. Yoshida, T. Kajino, T. Otsuka, Phys. Rev. C **74**, 034307 (2006).

[20] W. Hauser and H. Feshbach, Phys. Rev. **87**, 366 (1952).

[21] T. Nakagawa, S. Chiba, T. Hayakawa, T. Kajino, Atomic Data and Nuclear Data Table, **91**, 77 (2005).

[22] T. Yoshida, T. Suzuki, S, Chiba, T. Kajino, H. Yokomakura, K. Kimura, A. Takamura, H.

Hartmann, Astro. Phys. J. **686**, 448 (2008).

[23] T. Suzuki, M. Honma, K. Higashiyama, T. Yoshida, T. Kajino, T. Otsuka, H. Umeda, and K. Nomoto, Phys. Rev. C **79**, 061603(R) (2009).

[24] M. K. Cheoun, A. Bobyk, Amand Faessler, F. Simcovic and G. Teneva, Nucl. Phys. **A561**, 74 (1993) ; Nucl. Phys. **A564**, 329 (1993); M. K. Cheoun, G. Teneva and Amand Faessler, Prog. Part. Nuc. Phys. **32**, 315 (1994) ; M. K. Cheoun, G. Teneva and Amand Faessler, Nucl. Phys. **A587**, 301 (1995).

[25] Jouni Suhonen, *From Nucleons to Nucleus*, Springer, 2007.

[26] Y. K. Gambhir and Ram Raj, Phys. Rev. **162**, 1139 (1967).

[27] R. A. Meyer and R. P. Yaffe, Phys. Rev. **C 15**, 390 (1977).

[28] Kiran Jain and Ashok Kumar Jain, Phys. Rev. **C 45**, 3013 (1992).

[29] K. Gul, Phys. Rev. **C 79**, 044608 (2009).

[30] T. Hori *et al.*, Phys. Rev. **C 80**, 034306 (2009).

[31] E. Ydrefors, K. G. Balasi, T. S. Kosmas, J. Suhonen, Nucl. Phys. **A 866** (2011) 67-78, Erratum-ibid. **A 878** (2012) 1-2.

[32] E. Ydrefors, M. T. Mustonen, J. Suhonen, Nucl. Phys. **A 842** (2010) 33.

[33] T. W. Donnelly and W. C. Haxton, ATOMIC DATA AND NUCLEAR DATA **23**, 103 (1979).

[34] J. D. Walecka, *Muon Physics*, edited by V. H. Huges and C. S. Wu (Academic, New York, 1975), Vol II.

[35] N. Paar, D. Vretenar, T. Marketin, and P. Ring, Phys. Rev. **C 77**, 024608 (2008).

[36] S. M. Grimes *et al.*, Phys. Rev. **C 53**, 2709 (1996).

[37] A. Bortrungo and G. Co', Eur. Phys. J. **A24 S1**, 109 (2005).

[38] Giampaolo Co', Acta Physica Polonica **B 37**, 2235 (2006).

[39] Jonathan Engel, Phys. Rev. **C 57**, 2004 (1998).

[40] Myung-Ki Cheoun, Eunja Ha and T. Kajino, Phys. Rev. **C 83**, 028801 (2011).

[41] E. Kolbe, K. Langanke, G Martinez-Pinedo and P. Vogel, J. Phys. G **29**, 2569 (2003).

[42] M. T. Keil and G. G. Raffelt, Astrophys. J. **590**, 971 (2003).

[43] S. E. Woosley and A. Heger, Phys. Rep. **442**, 269 (2007).

[44] S. E. Woosley, in private communication (2012).

[45] M. B. Chadwick *et al.*, Nuclear Data Sheets **107**, 2931 (2006).

[46] K. Shibata *et al.*, J. Nucl. Sci. Tech. **48**, 1 (2011).

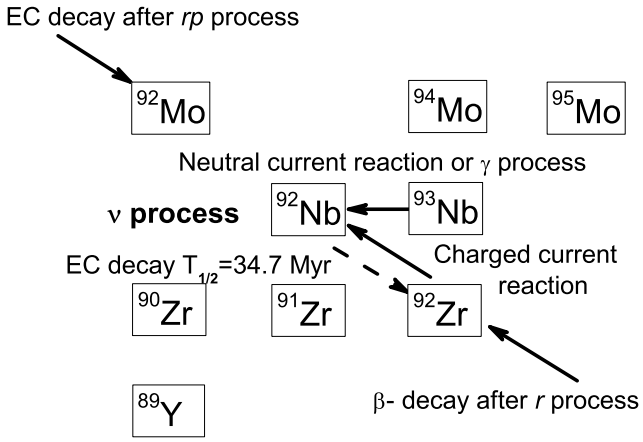

FIG. 1: Partial nuclear chart around ^{92}Nb indicating the main ν-process production from the $^{92}\mathrm{Zr}(\nu_e, e^-)^{92}\mathrm{Nb}$ charged-current (CC) and $^{93}\mathrm{Nb}(\nu(\bar{\nu}),\ \nu'(\bar{\nu})'\ \mathrm{n}\ )^{92}\mathrm{Nb}$ neutral-current (NC) reactions.

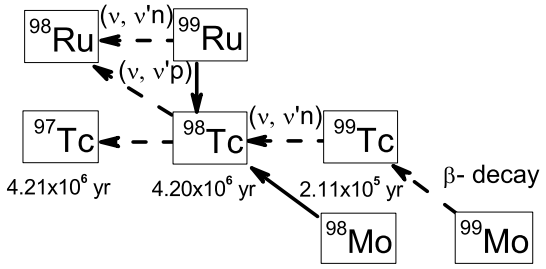

FIG. 2: Partial nuclear chart around ^{98}Tc indicating the main ν-process production from the $^{98}\mathrm{Mo}(\nu_e, e^-)^{98}\mathrm{Tc}$ CC reaction and the $^{99}\mathrm{Ru}(\nu(\bar{\nu}),\ \nu'(\bar{\nu})'\ \mathrm{p})^{98}\mathrm{Tc}$ NC reaction.

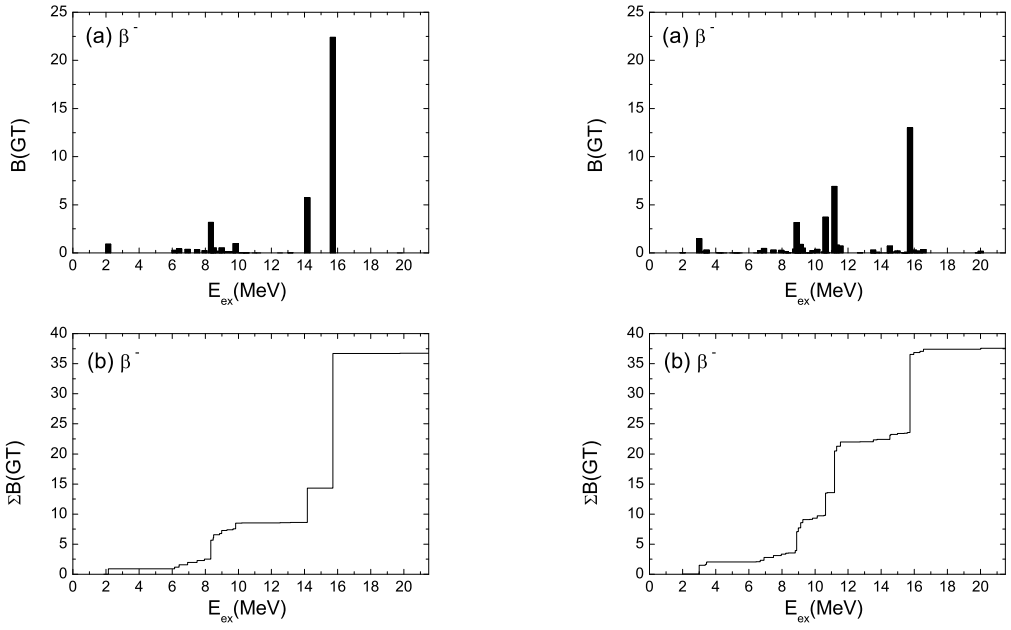

FIG. 3: GT(–) strength distributions for ^{92}Zr without *np* pairing (left) and with *np* pairing (right). The experimental Q value (= 2.005 MeV) between ^{92}Zr and ^{92}Nb should be subtracted from E_{ex}(MeV) to compare with the experimental data [36] measured w.r.t. the ^{92}Nb ground state.

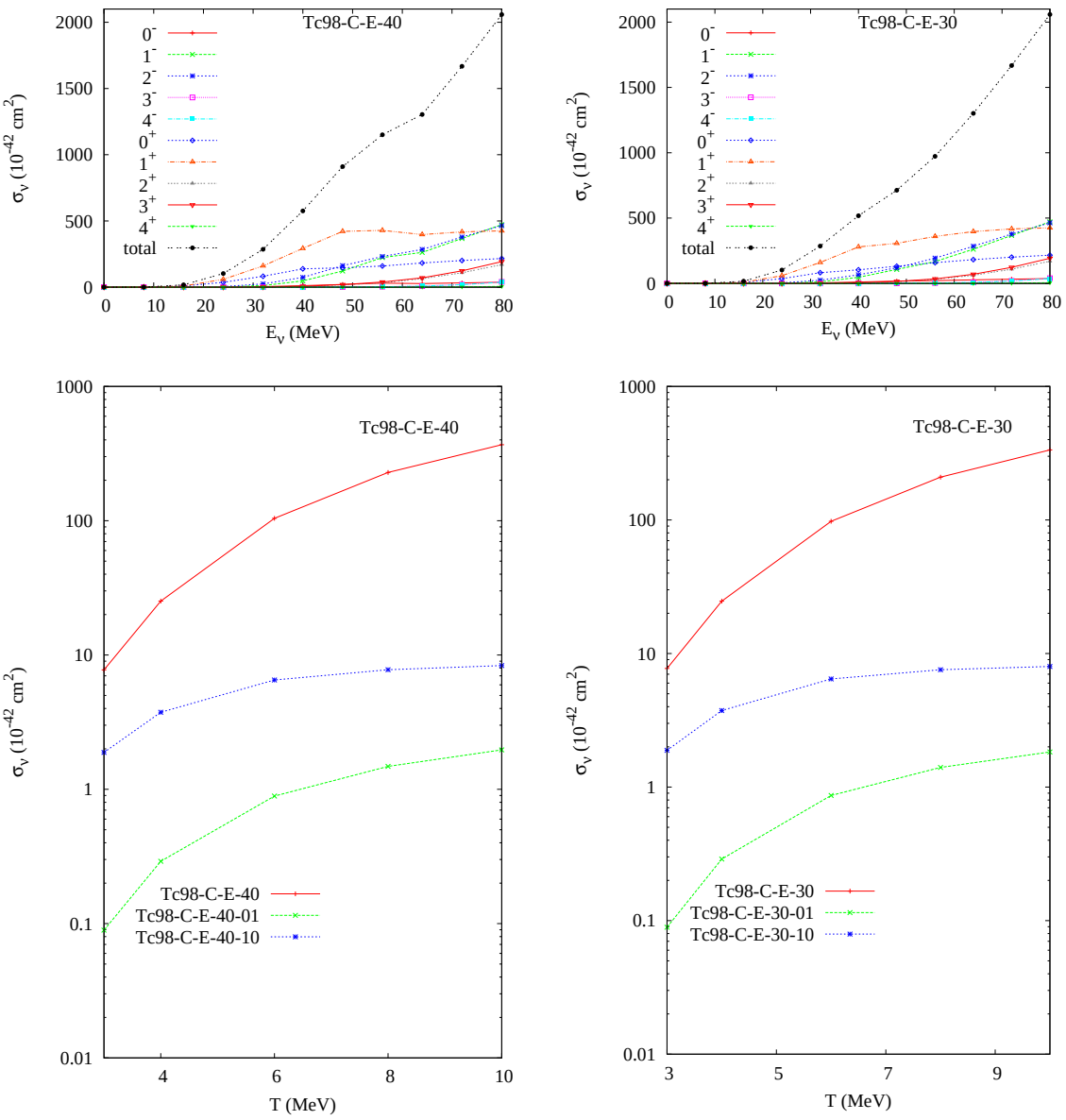

FIG. 4: (Color online) Energy (upper) and temperature (lower) dependent cross sections for the ^{98}Mo$(\nu_e, e^-)^{98}$Tc CC reaction. The contribution of each multipole transition is also presented along with their sum. Left and right panels are for a Coulomb cut at 40 or 30 MeV, respectively (see text for more explanation). The red curves in the lower panels are cross sections for the ^{98}Mo$(\nu_e, e^-)^{98}$Tc reaction. Blue and green curves are cross sections for proton and neutron emission channels from ^{98}Tc*, *i.e.* ^{98}Mo$(\nu_e, e^- p)^{97}$Mo and ^{98}Mo$(\nu_e, e^- n)^{97}$Tc.

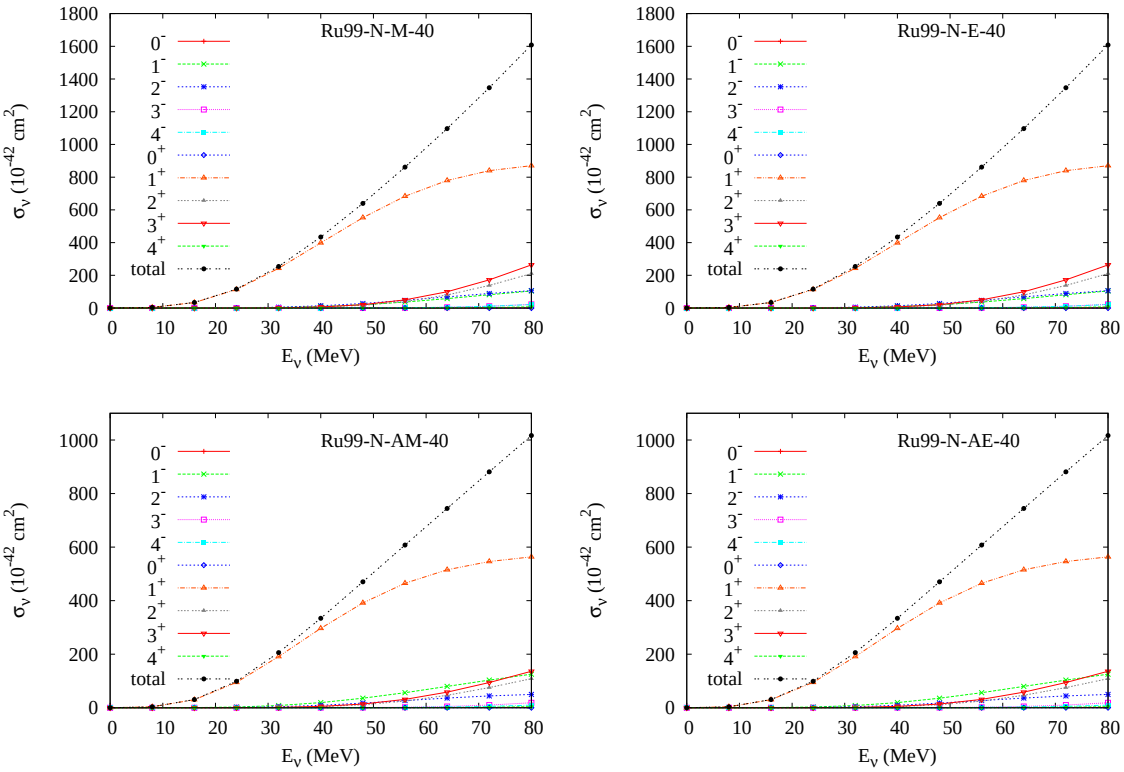

FIG. 5: (Color online) Energy dependent cross sections for NC reactions on ^{99}Ru. The upper two figures are for incident ν_μ (left) and ν_e (right). The lower two panels are for $\bar{\nu}_\mu$ (left) and $\bar{\nu}_e$ (right). Red curves are for the $^{99}\mathrm{Ru}(\nu(\bar{\nu}),\nu^{'}(\bar{\nu}^{'}))^{99}\mathrm{Ru}$ reaction. Blue and green curves are cross sections for neutron and proton emission from ^{99}Ru*, *i.e.* $^{99}\mathrm{Ru}(\nu(\bar{\nu}),\nu^{'}(\bar{\nu}^{'})n)^{98}\mathrm{Ru}$ and $^{99}\mathrm{Ru}(\nu(\bar{\nu}),\nu^{'}(\bar{\nu}^{'})p)^{98}\mathrm{Tc}$..

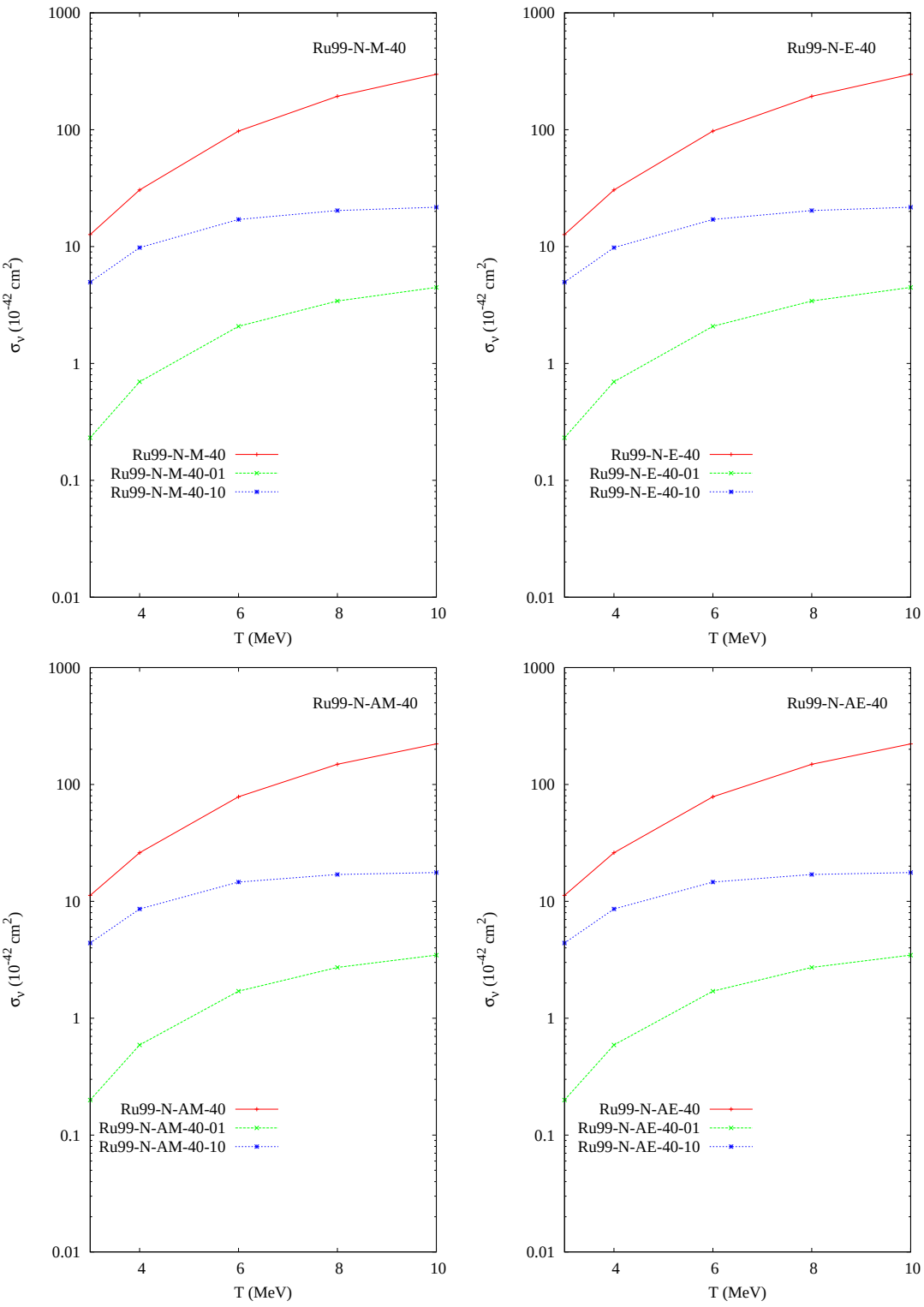

FIG. 6: (Color online) Temperature dependent cross sections for NC reactions on ^{99}Ru. The upper two figures are for incident ν_μ (left) and ν_e (right). The lower two panels are for $\bar{\nu}_\mu$ (left) and $\bar{\nu}_e$ (right). Red curves are for the $^{99}\mathrm{Ru}(\nu(\bar{\nu}),\nu^{'}(\bar{\nu}^{'}))^{99}\mathrm{Ru}$ reaction. Blue and green curves are cross sections for neutron and proton emission from ^{99}Ru*, *i.e.* $^{99}\mathrm{Ru}(\nu(\bar{\nu}),\nu^{'}(\bar{\nu}^{'})n)^{98}\mathrm{Ru}$ and $^{99}\mathrm{Ru}(\nu(\bar{\nu}),\nu^{'}(\bar{\nu}^{'})p)^{98}\mathrm{Tc}$.

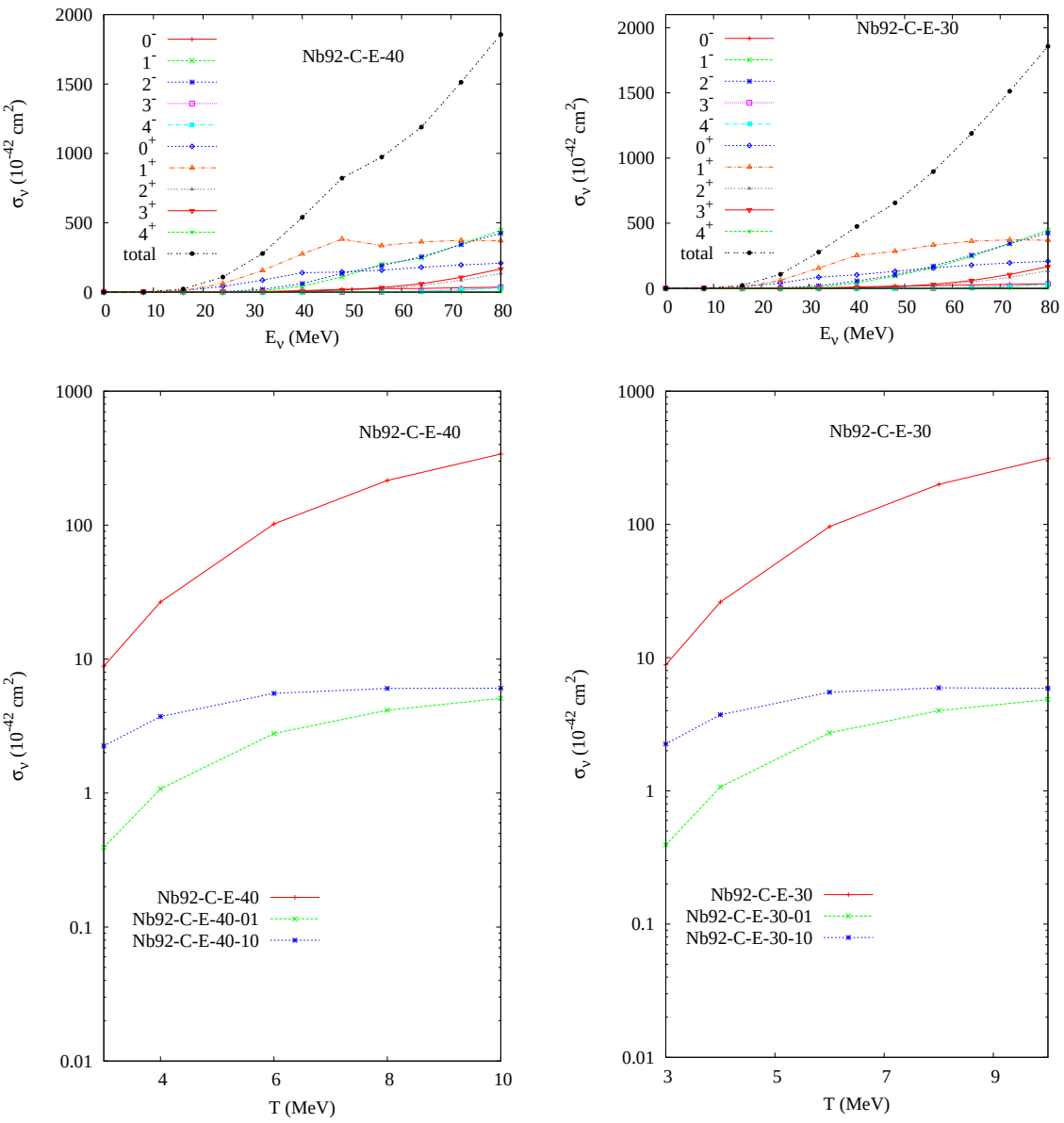

FIG. 7: (Color online) Energy and temperature dependent cross sections for the CC reactions on ^{92}Zr. Left (right) panels show the case of a 40 MeV (30MeV) Coulomb cut. Although results of both upper panels are slightly different, the thermally averaged cross sections shown in the lower panels are almost independent of the Coulomb cut. Red curves in the lower panels are cross sections for ^{92}Nb production, *i.e.* $^{92}\mathrm{Zr}(\nu_e, e^-)^{92}\mathrm{Nb}$. Blue and green curves are for proton and neutron emission, *i.e.* $^{92}\mathrm{Zr}(\nu_e, e^- p)^{91}\mathrm{Zr}$ and $^{92}\mathrm{Zr}(\nu_e, e^- n)^{91}\mathrm{Nb}$.

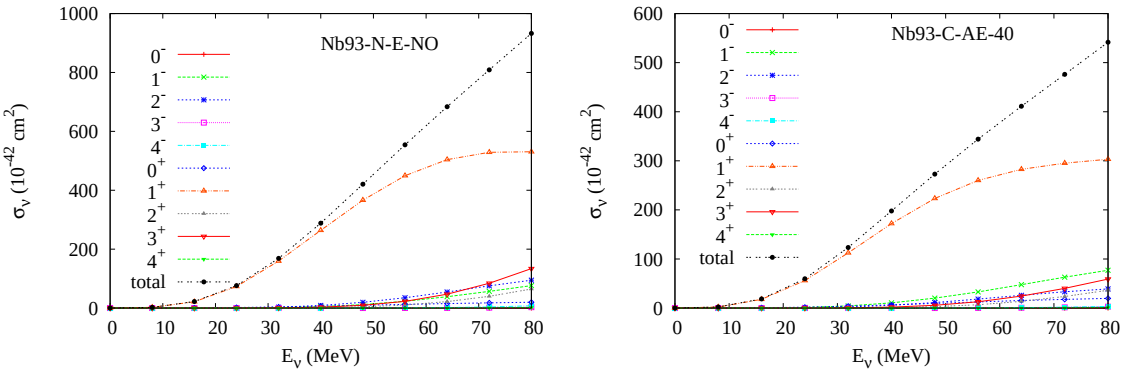

FIG. 8: (Color online) Energy dependent cross sections for the NC ^{93}Nb$(\nu(\bar{\nu}), \nu^{'}(\bar{\nu}^{'})n)^{92}$Nb reaction. The Left figure is for incident ν_e and the right is for $\bar{\nu}_e$.

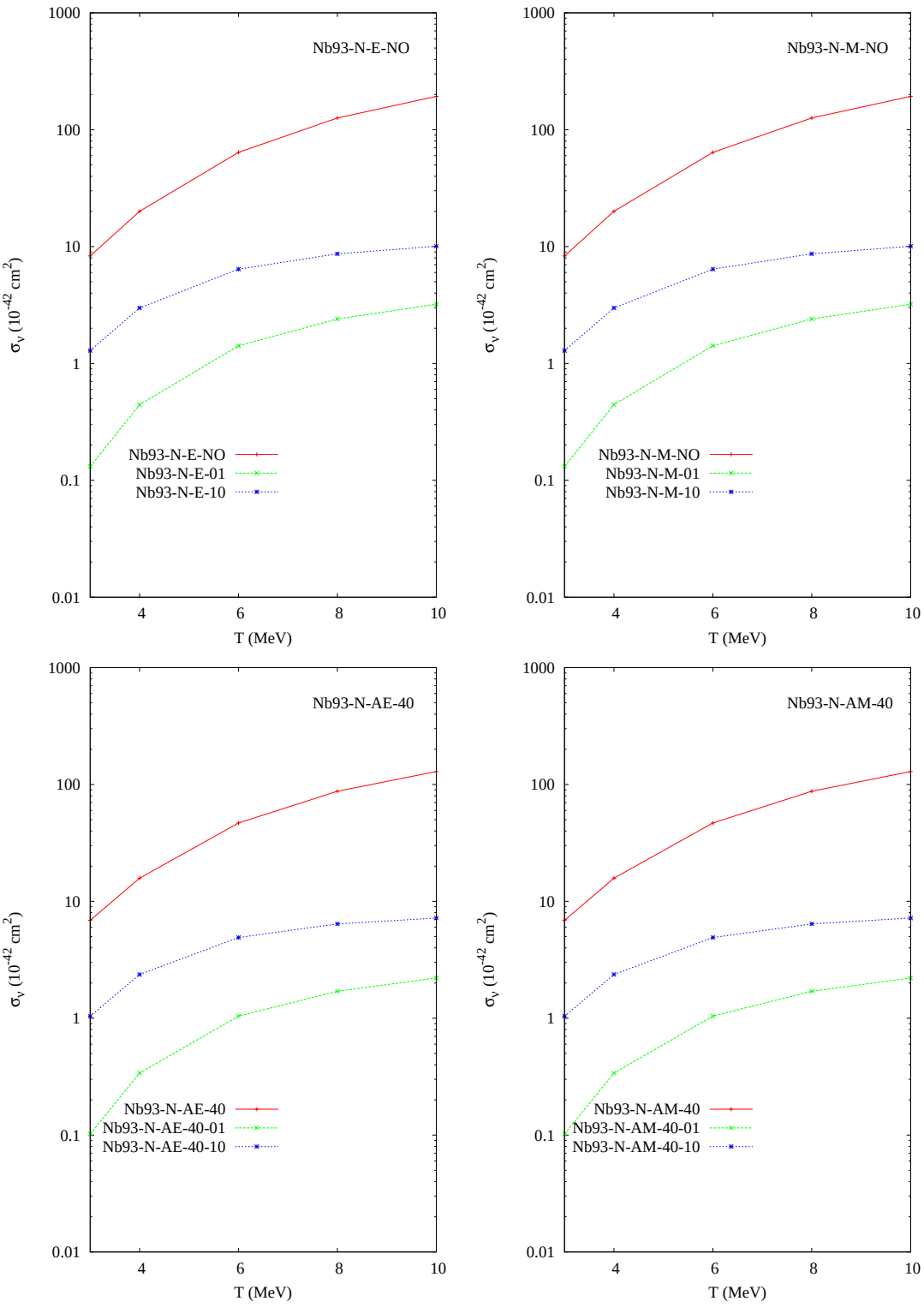

FIG. 9: (Color online) Temperature dependent cross sections for the NC reactions on ^{93}Nb. The upper two figures are for incident ν_e (left) and ν_μ (right). The lower two panels are for $\bar{\nu}_e$ (left) and $\bar{\nu}_\mu$ (right). Red curves are for the $^{93}\mathrm{Nb}(\nu(\bar{\nu}),\nu^{'}(\bar{\nu}^{'}))^{93}\mathrm{Nb}$ reactions. Blue and green curves are cross sections for proton and neutron emission from ^{93}Nb, *i.e.* $^{93}\mathrm{Nb}(\nu(\bar{\nu}),\nu^{'}(\bar{\nu}^{'})p)^{92}\mathrm{Zr}$ and $^{93}\mathrm{Nb}(\nu(\bar{\nu}),\nu^{'}(\bar{\nu}^{'})n)^{92}\mathrm{Nb}$.